AIAA JOURNAL
Vol. 57, No. 12, December 2019

Oscillating-Foil Turbine Operating at Large Heaving Amplitudes

M. Picard-Deland,* M. Olivier,† and G. Dumas‡
Laval University, Quebec City, Quebec G1V 0A6, Canada
and
T. Kinsey§
Lambda 2 Simulations, Quebec City, Quebec G1J 4K2, Canada

https://doi.org/10.2514/1.J058505

Oscillating-foil turbines have already proven to achieve efficiencies higher than 40% when operating at heaving amplitudes of the order of one chord with sinusoidal motions. In this 2D numerical parametric study, the energy extraction of an oscillating foil at a Reynolds number of 500,000 is maximized by prescribing large heaving amplitudes in combination with a modified pitching motion that imposes a sinusoidal evolution of the angle of attack. This allows to maintain a high efficiency of 44% for heaving amplitudes as large as 15 chords, meaning that a single large-amplitude turbine could efficiently exploit the same extraction window as about 10 smaller turbines having a standard one-chord heaving amplitude. By further modifying the pitching function to maintain a high angle of attack over a larger portion of the cycle, it is also possible to reach efficiencies as high as 49%. It is important to note that these impressive efficiencies are achieved at the cost of a significant energy input for the reversal of the foil at every half cycle, representing a potential practical challenge for a pitching controller.

Nomenclature

b	=	foil span, m
C_M	=	moment coefficient about the pitching axis
C_X	=	drag, or force coefficient in the x (incoming flow) direction
C_Y	=	force coefficient in the y (heaving) direction
$\overline{C_P}$	=	cycle-averaged power coefficient, $\overline{P}/((1/2)\rho U_\infty^3 bc)$
c	=	chord length, m
d	=	overall extent of the foil motion, m
f^*	=	reduced frequency, fc/U_∞
H_0	=	heaving amplitude, m
h	=	heaving position, m
P	=	instantaneous power exchanged with the flow, W
Re	=	Reynolds number, $U_\infty c/\nu$
T	=	cycle period, s
t	=	time, s
U_∞	=	upstream velocity, m/s
V_y	=	heaving velocity, m/s
α	=	angle of attack
α_0	=	angle-of-attack amplitude
β	=	shape parameter of the angle-of-attack function
η	=	efficiency, $\overline{P}/((1/2)\rho U_\infty^3 bd)$
θ	=	pitching angle
θ_0	=	pitching amplitude
$\dot{\theta}$	=	pitching velocity, rad/s
ϕ	=	phase shift between pitching and heaving motions

I. Introduction

RECENT studies [1,2] have shown that an oscillating foil could be used to efficiently extract kinetic energy from a flow instead of conventional rotating-blade turbines. This turbine concept could be particularly advantageous in certain environment where rotating blades at high speed are not efficient or not appropriate, such as in shallow rivers or tidal streams. However, unlike their horizontal-axis counterparts, oscillating-foil turbines (OFTs) rely on unsteady fluid dynamics and determining their optimal operating conditions require complex analysis. During the last decade, modern computational power has allowed to unveil the potential of this technology, which explains the renewed interest in trying to fully understand its energy-extracting mechanisms and maximize its theoretical performances for a variety of applications.

An OFT consists of a foil undergoing simultaneous heaving and pitching oscillating motions in a flow, extracting energy through the positive work done by the generated hydrodynamic forces. Its operating principle has been discussed in details in previous work [3]. The current effort in understanding and developing this turbine concept, pioneered by McKinney and DeLaurier in 1981 [4], was recently summarized in two comprehensive reviews by Young et al. [1] and Xiao and Zhu [2]. The oscillating motions can be either prescribed using a controller or mechanical constraints, or be induced by the flow itself in the case of a semipassive [5] or fully passive turbine [6]. Although it is crucial in designing an OFT to establish the way the motion of the foil is produced or constrained, this design decision is not required to assess the hydrodynamic efficiency of the turbine through numerical simulations. Thus, in this study, isolated single foils are considered, with their motions fully prescribed.

In 2008, Kinsey and Dumas [3] first investigated the power-extraction performances of a 2D oscillating foil under laminar flow conditions at a Reynolds number $Re = 1100$. Prescribed sinusoidal motions were used, with a heaving amplitude kept equal to the chord ($H_0/c = 1$) while the reduced frequency f^* and pitching amplitude θ_0 were varied to assess the efficiency in the $f^* - \theta_0$ parametric space. The good performances of the best case reported, which had an efficiency of 34%, were largely attributed to leading-edge vortex shedding (LEVS) caused by dynamic stall at every half cycle and its good synchronization with the foil's heaving motion, which dominates the energy extraction. This study eventually led to experiments on a 2 kW prototype mounted underneath a motor-powered boat on a lake at $Re = 500{,}000$ [7]. The hydrodynamic efficiency was estimated to be 30% for a single foil, after taking into account the mechanical losses in the power transmission, which was in good agreement with 3D numerical simulations performed at the prototype's operating conditions [8]. These simulations allowed to evaluate the 3D effects, with the conclusion that the decrease in efficiency compared with the 2D case is mostly due to a spanwise uncorrelation of the shed leading-edge vortex, thus yielding a less effective contribution of the well-timed LEVS at the foil tips. This observation suggests that it

Received 24 March 2019; revision received 9 July 2019; accepted for publication 13 September 2019; published online 15 October 2019.

*Research Professional, Laboratoire de Mécanique des Fluides Numérique, Département de Génie Mécanique; maxime.picard-deland.1@ulaval.ca.
†Assistant Professor, Laboratoire de Mécanique des Fluides Numérique, Département de Génie Mécanique; mathieu.olivier@gmc.ulaval.ca.
‡Professor, Laboratoire de Mécanique des Fluides Numérique, Département de Génie Mécanique; gdumas@gmc.ulaval.ca.
§Consultant; tkinsey@lambda2.ca.

would be difficult to develop an efficient technology that relies on this phenomenon.

In 2014, another 2D parametric study similar to that of 2008 was published by Kinsey and Dumas [9], but this time at the higher, more practical Reynolds number of 500,000 used in the 2011 trials. Larger heaving amplitudes of up to $H_0/c = 3$ were also studied, and efficiencies as high as 44% were obtained. Surprisingly, in these turbulent flow conditions and for the most efficient case found at $H_0/c = 1.5$, no dynamic stall or well-timed LEVS was observed, resulting in higher instantaneous forces and smoother power curve, but negative mean pitching contribution. The importance of reaching an optimal effective angle of attack (α) during the cycle was emphasized, and a mathematical relation based on this criterion was established to predict the optimal operating conditions at different H_0/c for imposed sinusoidal motions.

Drofelnik and Campobasso [10] conducted one of the most recent 3D numerical studies on the subject at $Re = 1{,}500{,}000$, using the same kinematic and geometric parameters as the previous 3D study by Kinsey and Dumas [8], with an aspect ratio $AR = 10$. They estimated that under these conditions, the 3D effects induce a 17% and 12% relative loss in power extraction compared with the 2D case, without and with endplates, respectively, and reiterated that relying on the contribution of well-timed LEVS would not be practical in a real-world application. Their results corroborated the ones obtained by Kinsey and Dumas [8] although a higher Reynolds number and a different turbulence model was used.

Kim et al. [11] recently did an extensive experimental parametric study at $Re = 50{,}000$, using constrained sinusoidal motions with H_0/c varying from 0.5 to 1.0. They used symmetrical foil cross sections such as a thin plate or an ellipse, ensuring a well-defined initiation of the LEVS. They investigated the impact of the aspect ratio and the use of different sizes of endplates, and drew similar conclusions as Kinsey and Dumas [8]: the delayed LEVS toward the tips of the foil accounts for most of the loss in performance with low aspect ratios, and endplates can significantly improve the efficiency (ranging from 31 to 38% depending on their size). Interestingly, they noted that the efficiency was not very sensitive to an increase in H_0/c, the extracted power increasing enough to compensate the larger swept area.

With the exception of [9], all of the studies presented above focused on an optimal case associated to H_0/c of the order of 1, despite the fact that it is generally observed that the extracted power increases with larger H_0/c. The apparently low interest in higher heaving amplitudes might be explained by the poor angle-of-attack profiles resulting from the imposed sinusoidal motions that are typically used for OFTs, quickly becoming impractical with increasing H_0/c as the heaving velocity gets much higher than that of the incoming flow. Furthermore, because most of the literature concentrates on cases featuring LEVS, it has become commonly accepted that this phenomenon is essential to achieve good performances. However, as concluded by the relevant 3D numerical studies, it would probably be unwise and impractical for an OFT to rely on well-timed LEVS, the latter being sensitive to the incoming flow velocity and turbulence intensity, and its benefits being weakened on span sections near the tips of a finite foil.

This paper proposes to explore the performances of OFTs operating at large heaving amplitudes. To avoid variations in the α profile through the parametric space, a sinusoidal angle of attack is directly prescribed through a modified pitching function. This idea was previously used for an OFT by Simpson [12] in an experimental study at $Re = 13{,}800$, although it was the heaving motion that was modified instead of the pitching motion to achieve similar results. The highest efficiencies reported were obtained with a sinusoidal angle of attack of amplitude $\alpha_0 = 39°$ for a heaving amplitude H_0/c between 0.75 and 1.23. Young et al. [13] later investigated the effect of varying the α profile for a turbine operating at $H_0/c = 1$ with a flow-driven frequency in a 2D parametric study at $Re = 1100$. They obtained efficiencies of up to 41% with a trapezoidal α profile of amplitude 40°, compared with a maximum of 30% when using sinusoidal motions. Finally, Lu et al. [14] studied similar α profiles at $Re = 10{,}000$ with $H_0/c = 0.8$ and found that, when limiting α_0 to 15°, the highest power extraction was achieved with a square-like α shape, which improved the LEVS synchronization.

In this 2D parametric study, the power extracted by an OFT at $Re = 500{,}000$ is investigated by varying its operating conditions. Heaving amplitudes as high as $H_0/c = 15$ are considered, effectively extending the relative portion of the cycle in which the foil is in its maximum power extracting state, reducing the time spent in the reversals. The objective of this work is not to present an exhaustive parametric study but rather a demonstration of the efficiency of the OFT concept operating at large heaving amplitudes. In that sense, the present paper should be viewed as an extension to our previous work also published in this journal [3,9].

II. Method

A. Foil Geometry and Kinematics

The OFT is represented by a 2D NACA 0020 undergoing a pitching motion $\theta(t)$ around a pitching axis located at 0.275 chord from the leading edge while undergoing a heaving motion $h(t)$ in a plane perpendicular to the incoming flow. This choice of pitching axis location is motivated by an ongoing experimental study and differs slightly from the one used in our previous work at $x_p/c = 0.33$ [9,15]. Figure 1 illustrates different positions of the foil during a cycle of period T. The angle of attack α is defined as the angle between the foil and the effective velocity, resulting from the vector addition of the upstream flow and heaving velocities, and is expressed as:

$$\alpha(t) = \arctan(-V_y(t)/U_\infty) - \theta(t) \tag{1}$$

where V_y is the heaving velocity corresponding to dh/dt and U_∞ is the upstream velocity. As mentioned in [9], the effective angle of attack as defined in Eq. (1) is not affected by the pitching velocity of the foil. The latter may be associated to an effective camber that does not affect the effective angle of attack $\alpha(t)$.

For OFTs operating at low heaving amplitudes, the pitching and heaving motions are traditionally sinusoidal and are expressed as:

$$\theta_{\text{trad}}(t) = \theta_0 \sin(\omega t) \tag{2}$$

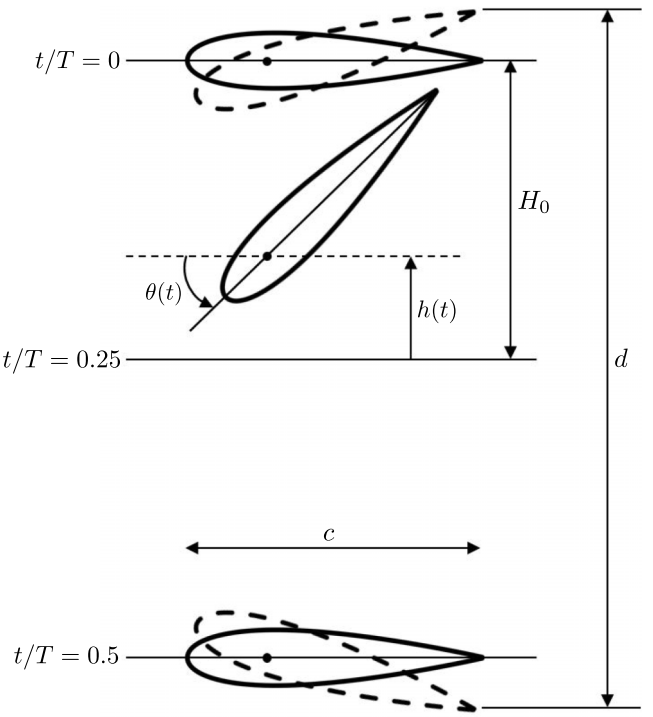

Fig. 1 Different positions of the foil during a cycle. The overall extent of the foil's motion *d* is used to determine the power extraction efficiency of the turbine.

$$h(t) = H_0 \sin(\omega t + \phi) \tag{3}$$

where θ_0 and H_0 are the pitching and heaving amplitudes, respectively, $\omega = 2\pi f$ is the angular frequency, and ϕ is the phase shift between the two oscillating motions, set to 90° for all the cases in this study. As shown in Fig. 2 with the motion curves for operating conditions close to the optimal case predicted by [9] at $H_0/c = 3$, these functions result in an increasingly distorted angle-of-attack profile at higher heaving amplitudes. A new function is therefore proposed in this work to prescribe the angle of attack as sinusoidal:

$$\alpha(t) = -\alpha_0 \sin(\omega t) \tag{4}$$

where α_0 is the angle-of-attack amplitude. To obtain the desired α profile, the expression for the modified pitching function is derived from Eqs. (1), (3), and (4):

$$\theta(t) = \arctan\left(-\frac{\omega H_0}{U_\infty}\cos(\omega t + \phi)\right) + \alpha_0 \sin(\omega t) \tag{5}$$

Note that, as discussed in [9], the instantaneous pitching angle might reach values larger than 90° in order to achieve optimal effective angle-of-attack amplitudes α_0 at large heaving amplitudes (see Fig. 2).

In this study, the heaving function is maintained sinusoidal, as defined in Eq. (3). The three main parameters that define the parametric space are thus the heaving amplitude normalized by the chord H_0/c, the reduced frequency $f^* = fc/U_\infty$, and the amplitude of the angle-of-attack profile α_0 (or maximum angle of attack reached during the oscillation cycle).

B. Power Extraction

Both the heaving and pitching motions of the foil contribute to its energy exchange with the flow, and the instantaneous power is expressed as:

$$P(t) = P_Y(t) + P_\theta(t) = Y(t)V_y(t) + M(t)\dot{\theta}(t) \tag{6}$$

where Y is the force acting on the foil in the heaving direction and M is the moment about the pitching axis. The dimensionless power coefficient of the turbine is defined as:

$$\overline{C_P} = \frac{\overline{P}}{(1/2)\rho U_\infty^3 bc} \tag{7}$$

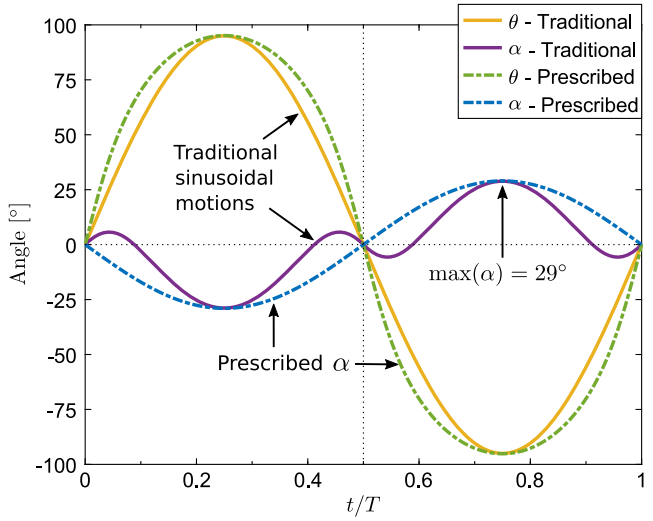

Fig. 2 Comparison between a traditional sinusoidal pitching motion of amplitude $\theta_0 = 95°$ and a prescribed sinusoidal angle-of-attack profile of amplitude $\alpha_0 = 29°$, with $H_0/c = 3$ and $f^* = 0.12$.

where $\overline{P}$ is the cycle-averaged power extracted by the foil, ρ is the fluid density, and b is the foil span. In a similar manner, the heaving force coefficient is defined as

$$C_Y(t) = \frac{Y(t)}{(1/2)\rho U_\infty^2 bc} \tag{8}$$

and the moment coefficient as

$$C_M(t) = \frac{M(t)}{(1/2)\rho U_\infty^2 bc^2} \tag{9}$$

In the case of 2D simulations, the value of these coefficients is given per unit depth. Multiple definitions for the efficiency η have been used in the literature for OFTs, as noted in [9]. The one used here is the most stringent one, taking into account the motion of any point of the foil in the definition of the swept area, and is expressed as:

$$\eta = \frac{\overline{P}}{(1/2)\rho U_\infty^3 bd} \tag{10}$$

where d is the overall extent of the foil motion shown in Fig. 1.

C. Numerics

Unsteady Reynolds-averaged Navier–Stokes (URANS) simulations have been run with the commercial software CD-Adapco STAR CCM+ v11.04.010, using an incompressible segregated flow solver together with the SIMPLE algorithm and the one-equation Spalart–Allmaras turbulence model [16], with a modified production term (modified deformation option) [17] as used previously by Kinsey and Dumas [9,15]. Second-order schemes are used for pressure, momentum, turbulent quantities, and time discretization.

The dimensions of the domain, shown in Fig. 3, depend on the value of the heaving amplitude H_0/c to account for the large variation in the size of the swept area between cases at $H_0/c = 1$ and $H_0/c = 15$. This is essential to ensure a comparable confinement of the turbine with respect to the boundary conditions. Indeed, Gauthier et al. [18] observed that the power extracted by an OFT increases linearly with the blockage ratio when the latter is inferior to 40%. Here, a constant heavingwise blockage of 1% has been chosen and the domain dimensions in the flow direction have been scaled accordingly, as shown in Table 1. Uniform velocity inlet and zero static pressure outlet are used upstream and downstream, respectively, with a modified viscosity ratio at inlet of $\tilde{\nu}/\nu = 3$ corresponding to a turbulent viscosity ratio of 0.2. Symmetry conditions are used for the top and bottom boundaries. The flow domain is initialized with a uniform field corresponding to the inlet conditions.

The overset mesh function of STAR-CCM+ is used to superimpose the moving foil's mesh with the static background mesh. The moving region is a 50,000-cell structured mesh generated with ANSYS ICEM v17.0, using an O-grid that extends between 0.5 and 0.8 chord radially from the NACA 0020 profile, with 382 nodes along the wall and a first cell height of 6.5×10^{-5} chord. The resulting $y+$ has been verified to be of order $\mathcal{O}(1)$ over most of the cycles for all simulations. Although the same moving mesh is used for all cases, the hexagonal background mesh, generated with STAR-CCM+, is adjusted with H_0/c to ensure that the blockage effect is the same for all simulations.

Table 1 Domain dimensions, normalized with the chord length and illustrated in Fig. 3, along with space and time resolution for different heaving amplitudes

H_0/c	D_y	D_{up}	D_{down}	Total cells	TS/cycle
1	100	20	50	149,000	2,000
3	300	60	150	220,000	2,000
5	500	100	300	250,000	3,000
10	1,000	200	500	397,000	5,000
15	1,500	300	700	800,000	8,000

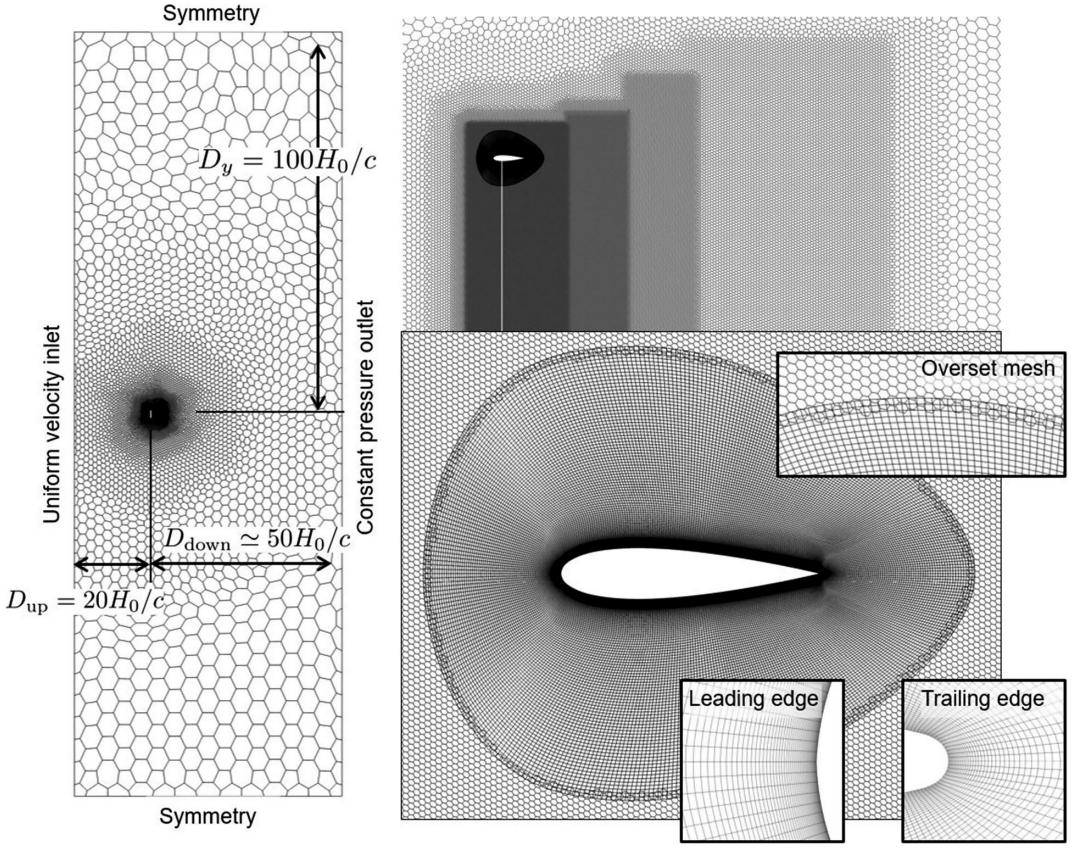

Fig. 3 Domain size (normalized with the chord length), boundary conditions, and mesh representation taken from a case with $H_0/c = 5$ with foil in its upper heaving position. The vertical white line on the left and top portions of the figure represents the extent of the pitching axis heaving motion.

Different zones have been defined to control the mesh density in the heaving region as well as in the wake of the turbine, as shown in Fig. 3, resulting in the number of cells given in Table 1.

The number of time steps (TS) per cycle has also been increased with H_0/c to account for the larger velocities encountered at larger heaving amplitudes in order to preserve a similar Courant number. The number of iteration (IT) per time step has been fixed to 25, which is sufficient to reach stabilized instantaneous force coefficients (within 0.01%). To accelerate the computations in the transient period before reaching a periodic flow solution, the six first cycles are simulated using half the time resolution given in Table 1 and with only 10 IT/TS.

D. Cycle-to-Cycle Convergence

The evolution of the mean power coefficient $\overline{C_P}$ with the simulation cycles is monitored to ensure that a satisfying statistical convergence is achieved for all cases. Different convergence patterns have been identified by Kinsey and Dumas [9], such as a $\overline{C_P}$ converging monotonically to a constant value or approaching an asymptote (type 1), a $\overline{C_P}$ oscillating around an identifiable average value due to complex vortex shedding that affects the foil differently from cycle to cycle (type 2), or a $\overline{C_P}$ with chaotic variations on a large time scale due to the foil interacting with its own wake (type 3). In this study, a type 1 behavior has been observed for most of the simulations, whereas different convergence patterns are otherwise clearly identified in Sec. III.A. The few simulations displaying a type 2 convergence have been run long enough to confidently extract an averaged $\overline{C_P}$ value over multiple cycles, and cases displaying a type 3 convergence have been excluded from the analysis. Interested readers can refer to [9] for illustrations of these three types of convergence.

For large heaving amplitudes, convergence is slower because the domain, the number of cells, and the time resolution are larger. For most of these simulations, the $\overline{C_P}$ evolution has been monotonic with a common asymptotic type 1 pattern. An estimation of the asymptote is then computed to quantify $\overline{C_P}$. Some cases that have been run for a large number of cycles have been used to model the $\overline{C_P}$ convergence pattern with a law of the type:

$$\overline{C_P} = \frac{A}{1 + B\exp(C(N + D))} + E \tag{11}$$

where N is the number of cycles and A to E are curve fitting parameters, E being the value of the asymptote. A nonlinear least square regression has then been used to optimize these parameters for the $\overline{C_P}$ convergence curve of other cases, effectively predicting a value for $N \to \infty$. An example of such a prediction is given in Fig. 4 for a type 1 convergence. When this method is used, the values of

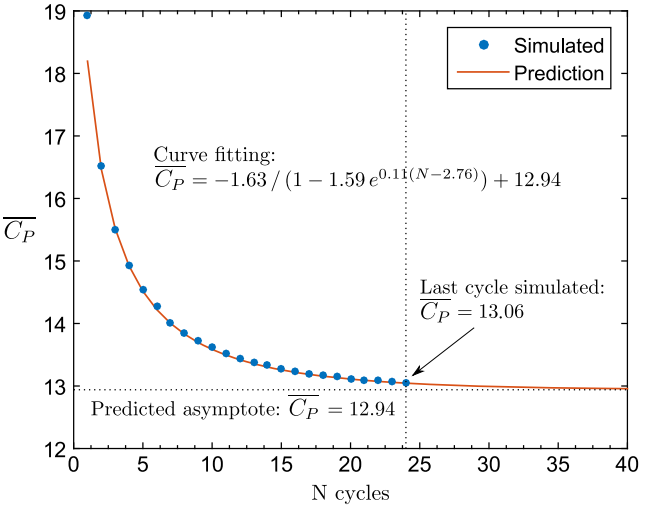

Fig. 4 Prediction of an asymptote value for the $\overline{C_P}$ convergence curve of a case at $H_0/c = 15$ with $f^* = 0.07$ and $\alpha_0 = 13°$. Type 1 convergence.

Table 2 Numerical parameters and results for validation case $H_0/c = 1$, $f^* = 0.16$, $\theta_0 = 75°$

Case name	Cells (mov.)	Cells (back.)	TS/cycle	IT/TS	$\hat{C}_Y$	$\hat{C}_M$	$\overline{C_P}$
Ref. [15]	N/A	42,200	2,000	N/A	3.168 (−0.90%)	0.613 (−0.09%)	1.023 (−1.31%)
Coarse mesh	30,000	67,000	2,000	25	3.137 (−1.88%)	0.607 (−0.92%)	1.018 (−1.82%)
Standard	**50,000**	**99,000**	**2,000**	**25**	**3.197**	**0.613**	**1.037**
Low IT	50,000	99,000	2,000	10	3.222 (0.78%)	0.619 (0.91%)	1.037 (0.08%)
High IT	50,000	99,000	2,000	50	3.195 (−0.08%)	0.613 (−0.03%)	1.037 (0.06%)
Coarse TS	50,000	99,000	2,000	25	3.220 (0.73%)	0.614 (0.20%)	1.036 (−0.03%)
Fine TS	50,000	99,000	4,000	25	3.187 (−0.33%)	0.613 (0.04%)	1.037 (0.06%)
Fine mesh	73,000	152,000	2,000	25	3.207 (0.30%)	0.613 (0.06%)	1.039 (0.24%)

The percentages are differential values relative to the standard resolution in bold.

efficiency, force, and power coefficients are scaled accordingly (i.e., with the ratio of the predicted $\overline{C_P}$ to the one obtained at the last simulated cycle).

E. Validation

To validate the numerical method presented above, which differs slightly from the ones used previously by Kinsey and Dumas [3,9,15], multiple simulations have been run for the test case of a sinusoidally constrained NACA 0015 with a pitching axis located at 0.33 chord from the leading edge, operating at $H_0/c = 1$ with pitching amplitude $\theta_0 = 75°$ and phase $\phi = 90°$ at $Re = 500{,}000$. Results are compared with the ones reported by Kinsey and Dumas [7,15].

The specific case $f^* = 0.16$, free of LEVS and thus with dynamics similar to the majority of the cases of interest in this study, is chosen to investigate independence of time and space discretization. For both the moving (mov.) and the background (back.) meshes, a coarser and a finer version than the standard case described in Sec. II.C has been created. Simulations have also been run with a lower and higher number of time steps per cycle and iterations per time steps. Table 2 summarizes the resulting peak heaving force coefficient ($\hat{C}_Y$), peak moment coefficient ($\hat{C}_M$), and mean power coefficient ($\overline{C_P}$), along with the corresponding reference data from Kinsey and Dumas [15]. Note that all validation cases have been simulated until a satisfying $\overline{C_P}$ convergence is achieved, as described in Sec. II.D.

Although the impact on the $\overline{C_P}$ is small (less than 0.1%), increasing the time resolution or number of iterations per time step both tend to decrease the peak forces, but to a very limited extent when comparing the standard (2000 TS/cycle, 25 IT/TS) and finer parameters (4000 TS/cycle or 50 IT/TS). For a given time resolution and number of iterations per time step, the peak forces and $\overline{C_P}$ values increase with mesh resolution. A similar observation is made on the instantaneous curves provided in Fig. 5, which also show a good match with the results from [15]. The difference between the standard and fine mesh being very small, it is accepted that the results are independent from time and space resolution with the standard parameters.

With the selected numerical resolution, the same test case has then been run at frequencies ranging from $f^* = 0.04$ to 0.18 to compare the results with experimental data [7], as well as the 2D and 3D numerical validation study by Kinsey and Dumas [15], which used a different solver and methodology. Figure 6 shows again a good agreement between the 2D efficiencies of the present methodology and those obtained in [15], apart from the case $f^* = 0.10$, one with a critical LEVS contribution that marked the beginning of an efficiency plateau in the former study. Here, this plateau begins with $f^* = 0.12$, after which the contribution of the LEVS (disappearing totally at $f^* = 0.16$) becomes no longer sufficient to compensate the faster pitch reversals at higher frequencies (see Sec. III.B for a detailed analysis of the energy extraction contributions). The results of the present study match the trend of the referenced numerical and experimental results, that is, a progressive increase of efficiency with the reduced frequency until a plateau is reached. The 2D predictions for high-performance cases converge to a higher efficiency plateau, which is expected because 2D simulations do not account for the losses at the wing tips. Note that the foil in the experimental and 3D numerical studies had endplates and an aspect ratio $AR \equiv (b/c) = 7$.

III. Results

A. Performance of the Optimal Cases

More than 150 cases have been simulated in order to characterize the $f^* - \alpha_0$ parametric space around the optimal operating conditions for $H_0/c = 1$, 3, 5, 10, and 15 at $Re = 500{,}000$. With the prescription of a sinusoidal angle of attack, maximum efficiencies of

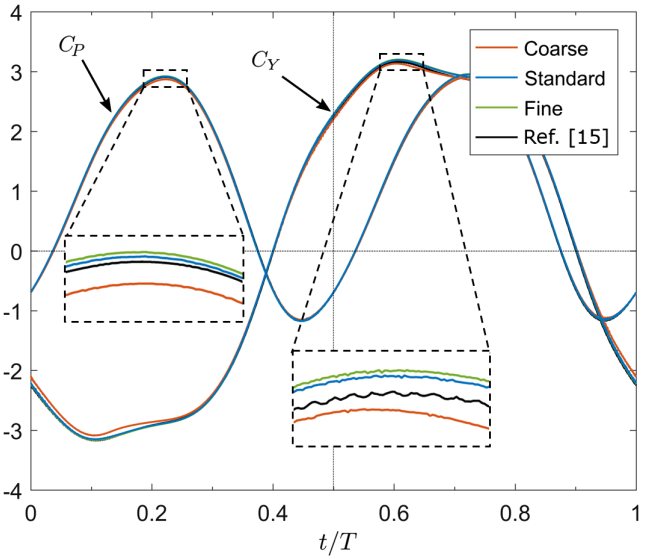

Fig. 5 Instantaneous C_P and C_Y curves for validation case $H_0/c = 1$, $f^* = 0.16$, $\theta_0 = 75°$ with different mesh sizes, along with results from Kinsey and Dumas [15].

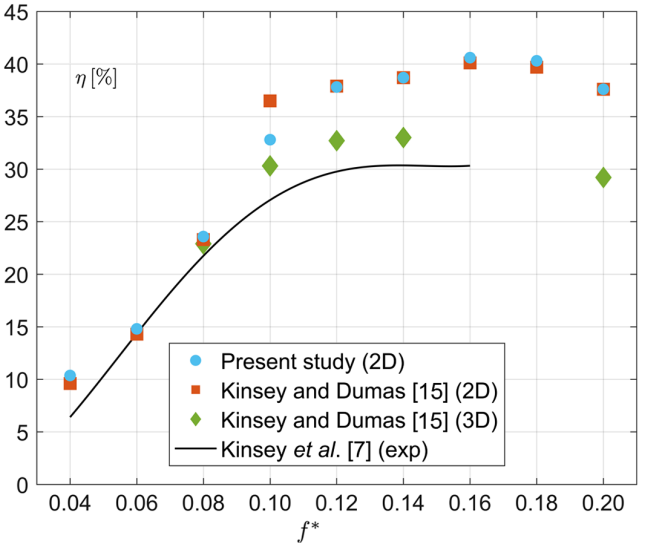

Fig. 6 Resulting efficiency at different reduced frequencies for the validation case $H_0/c = 1, \theta_0 = 75°$. The experimental curve is a minimal bound to the estimated hydrodynamic efficiencies in [7].

Table 3 Kinematic parameters, turbine drag, and mean power extraction of the most efficient cases found at each heaving amplitude studied

H_0/c	f^*	α_0, °	Max (V_y/U_∞)	Max $(\dot{\theta}c/U_\infty)$, °	d/c	$\overline{C_X}$	$\overline{C_{P_\theta}}$	$\overline{C_P}$	η, %
1	0.14	37	0.88	77	2.72	2.135	−0.317	1.141	42.0
1	0.14	49	0.88	87	2.83	3.043	−0.135	1.258	44.5
3	0.12	27	2.26	118	6.70	5.320	−0.588	3.000	44.8
5	0.105	21	3.30	139	10.70	8.020	−0.640	4.810	44.9
10	0.08	18	5.03	154	20.71	15.424	−0.547	9.214	44.5
15	0.07	15	6.60	173	30.73	22.765	−0.544	13.489	43.9

Here, case $H_0/c = 1$, $f^* = 0.14$, $\alpha_0 = 49°$ is the only one featuring LEVS.

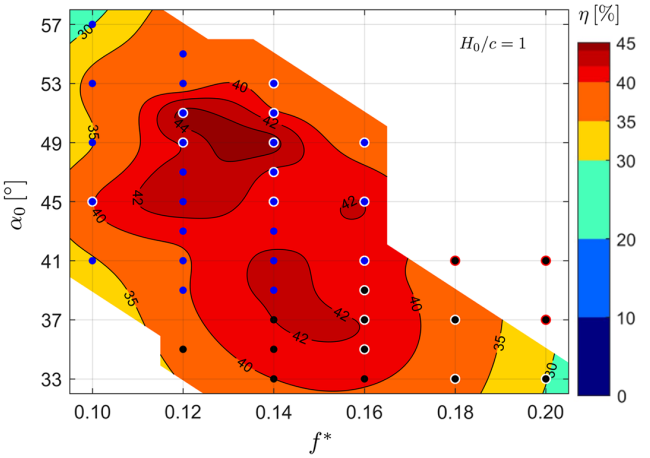

Fig. 7 Isocontours of efficiency in the $f^* - \alpha_0$ parametric space for $H_0/c = 1$. Simulated points are shown. A blue point indicates the occurrence of LEVS, whereas a point circled in white and a point circled in red represent type 2 and type 3 convergence, respectively.

44–45% are reached for all heaving amplitudes studied, as shown by the efficiency contours provided in Figs. 7 and 8. The specific parameters and performance metrics of the most efficient cases are reported in Table 3.

As shown in Fig. 9, the optimal parametric region moves toward lower values of f^* and α_0 and its size decreases as H_0/c increases, the performance of the turbine becoming more sensitive to variations in the kinematic parameters. However, maintaining a high efficiency with such a large extraction window implies that the foil extracts about 10 times more power operating at $H_0/c = 15$ than when operating with the same efficiency at $H_0/c = 1$. This can be seen by comparing the values of mean power coefficient $\overline{C_P}$ in Table 3. It is important to note that the size of the extraction window d is not exactly proportional to H_0/c, being more affected by the foil's rotating motion when H_0/c is small and the optimal value of α_0 is large (see Fig. 1). The efficiency is thus proportional to $\overline{C_P}/d$, as detailed in Eq. (10). Furthermore, the lower optimal kinematic parameters f^* and α_0 found at higher heaving amplitudes do not compensate for the larger distance that the foil needs to travel, and the resulting maximum linear and angular velocities reached during the cycle increase significantly with H_0/c for the efficient cases. The

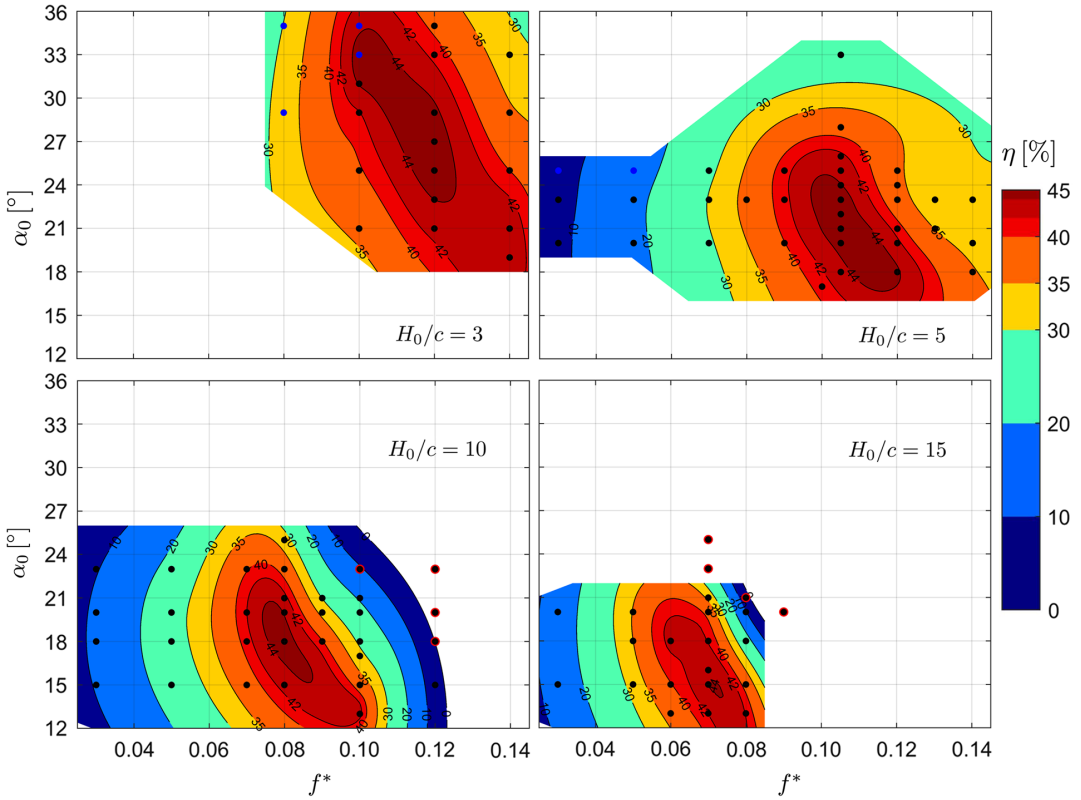

Fig. 8 Isocontours of efficiency in the $f^* - \alpha_0$ parametric spaces associated to high heaving amplitudes. Simulated points are shown. A blue point indicates the occurrence of LEVS, whereas a point circled in red represents a type 3 convergence.

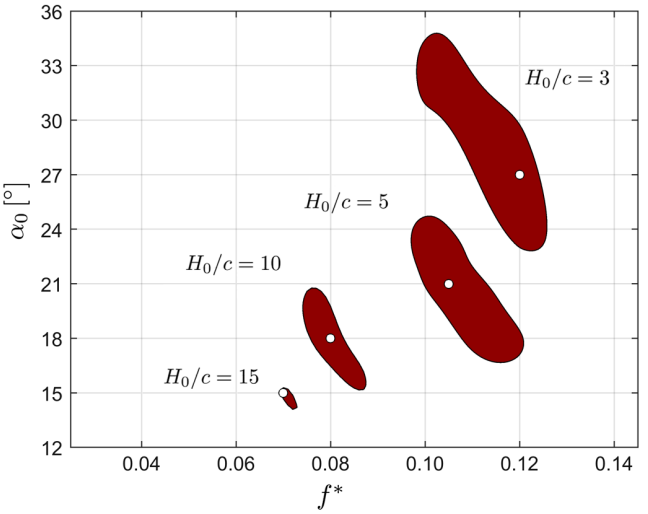

Fig. 9 Overall view of the high-performance regions in the $f^* - \alpha_0$ parametric space represented with iso-surfaces of $\eta = 44\%$ for various values of heaving amplitudes. White points correspond to the most efficient cases.

associated accelerations, notably the angular acceleration, could represent a mechanical challenge in practice for the pitch controller.

B. Low Heaving Amplitude and LEVS

Although LEVS is sometimes present at $H_0/c = 1$, it was absent from most of the cases at higher heaving amplitudes, only occurring when combining low H_0/c, low f^*, and high α_0. One expects indeed that a well-timed LEVS, which induces a pitching moment that helps the rotation of the foil at every half cycle, becomes less important as H_0/c increases and the time spent during reversals decreases. Interestingly, a high efficiency of 42% is obtained without LEVS even at the low heaving amplitude of $H_0/c = 1$. A comparison of two cases leading to 42% efficiency is shown in Fig. 10, one featuring LEVS and the other one without LEVS. In the case with no LEVS, the boundary layer is close to separation during reversals, but stays attached to the foil unlike the case featuring LEVS. This allows to maintain a smooth and high-amplitude force coefficient C_Y during the portion of the cycle at which the heaving velocity V_y is large, although the two curves are not perfectly synchronized. The resulting positive peak of the instantaneous power coefficient $C_P(t)$ is larger in the absence of LEVS, which compensates for the negative mean pitching contribution $\overline{C_{P_\theta}}$.

When including cases with a type 2 convergence, and thus an unstable $\overline{C_P}$, an even higher efficiency of 44.6% is found at $H_0/c = 1$, with $f^* = 0.14$ and $\alpha_0 = 49°$. In this case, the timing of the LEVS varies from cycle to cycle, yielding an efficiency that oscillates between 42 and 46%. Type 2 convergence has not been observed in this study for any simulation ran at higher H_0/c, whereas LEVS has been observed only for a few cases at $H_0/c = 3$ and 5, as indicated by the blue dots in Fig. 8.

One can note that type 3 convergence (chaotic: red points in Figs. 7 and 8) occurs away from the optimal operating conditions. This is not coincidental; increasing the angle-of-attack amplitude α_0 and the reduced frequency f^* leads to a strong interaction of the foil with its own wake [9], yielding unstable performances.

C. Impact of the Kinematic Parameters on Energy Extraction

For the reasons mentioned in Sec. II.A, prescribing the angle of attack rather than the pitch angle becomes essential at high heaving amplitudes such as $H_0/c = 5$, but the impact is somewhat limited for low values such as $H_0/c = 1$, where high efficiencies had already been achieved with sinusoidal motions. Kinsey and Dumas [9] reported their optimal case at $H_0/c = 1.5$ and observed a drop in the performances when further increasing the heaving amplitude.

In the present study, at $H_0/c = 3$, a sinusoidal α profile leads to smoother instantaneous force and moment coefficients, which ultimately improve performances. To illustrate this, Fig. 11 compares the results between two efficient cases: one with a sinusoidal pitching motion $\theta(t)$ and the other with a prescribed sinusoidal angle of attack $\alpha(t)$. The kinematic parameters of both cases are chosen such that the maximum angle of attack reached during a cycle is $\alpha_0 = 29°$ at a reduced frequency of $f^* = 0.12$, resulting in the instantaneous $\alpha(t)$ and $\theta(t)$ curves previously illustrated in Fig. 2. Note that the scales are different between Figs. 10 and 11. With a prescribed angle of attack, C_Y is maintained at a high value for a larger portion of the cycle,

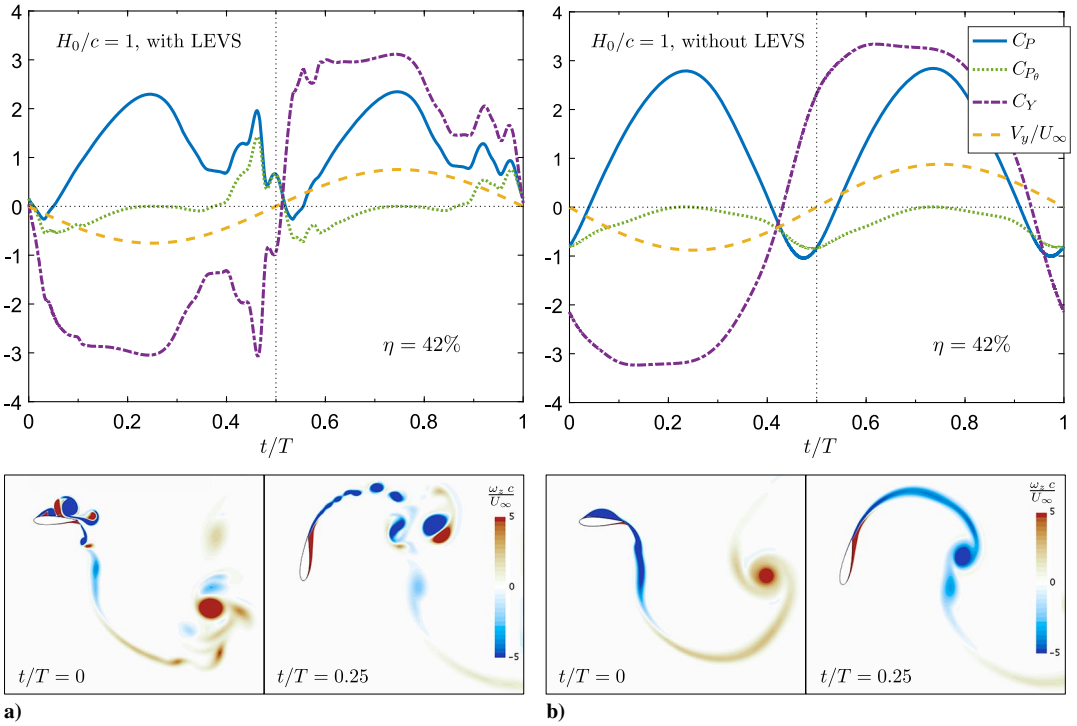

Fig. 10 Comparison of the instantaneous power contributions and vorticity fields between two high-performance cases of same efficiency $\eta = 42\%$ at $H_0/c = 1$, with or without LEVS. a) $f^* = 0.12, \alpha_0 = 47°$; b) $f^* = 0.14, \alpha_0 = 37°$.

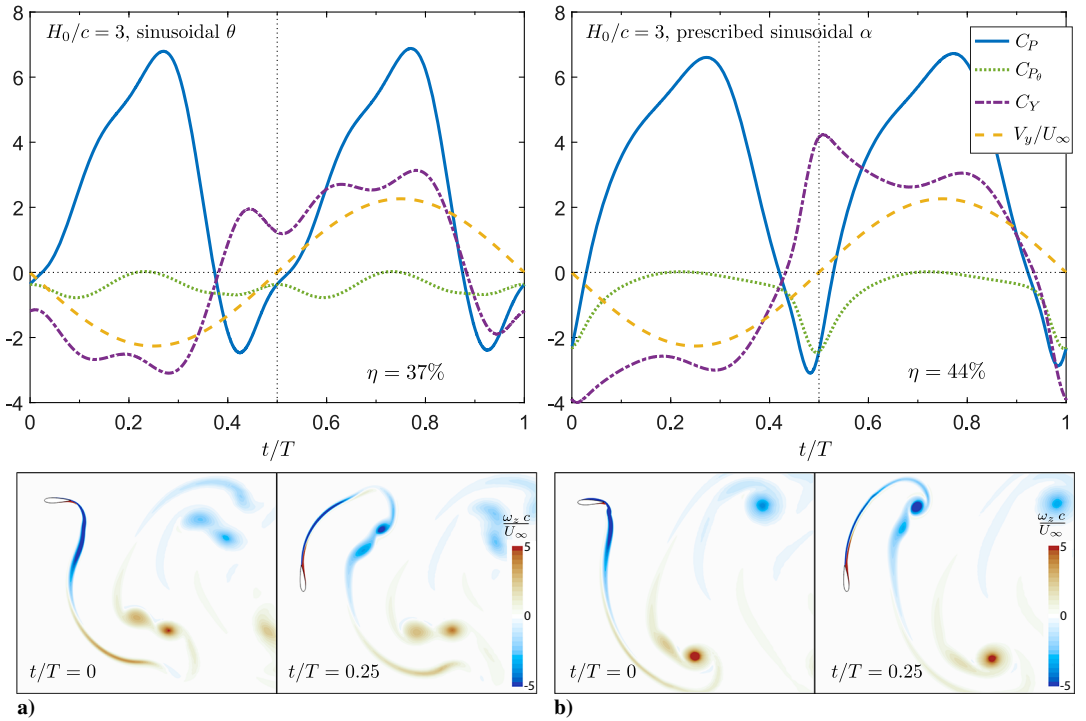

Fig. 11 Comparison between two efficient cases at $H_0/c = 3$ and $f^* = 0.12$ sharing same $\alpha_0 = 29°$, whose $\alpha(t)$ and $\theta(t)$ curves are shown in Fig. 2: a) sinusoidal motions with $\theta_0 = 95°$ and b) prescribed sinusoidal angle of attack with $\alpha_0 = 29°$.

resulting in a fuller $C_P(t)$ profile and a higher efficiency (44% compared with 37% for the sinusoidal $\theta(t)$ case). The pitching power contribution C_{P_θ} tends toward a steady null value when the foil is at its maximal angle of attack (i.e., around $t/T = 0.25$ and $t/T = 0.75$), although turning into an intense negative peak during reversals due to the higher pitching velocity $\dot{\theta}$ (see Fig. 2).

Let us now compare the optimal cases at different heaving amplitudes listed in Table 3, and thus with varying values of f^* and α_0. The force and power coefficient profiles are found to be similar to that of the case shown in Fig. 11b for all efficient cases without LEVS at $H_0/c = 3$ and 5. For $H_0/c = 10$ and 15, the higher velocities amplify the unsteady effects and the intensity of the variations of the instantaneous C_Y, as shown in Fig. 12 for $H_0/c = 10$. This results in a drop of the $C_P(t)$ slope after the reversals (i.e., around $t/T = 0.1$ and 0.6) when comparing to cases at lower heaving amplitudes. Nevertheless, the magnitude of the C_P curve increases with H_0/c, as seen with the different scales used in Figs. 10–12. This is due to the higher heaving velocity V_y, but also to a slight increase in the amplitude of the C_Y curve, both leading to a higher heaving power coefficient $\overline{C_{P_Y}}$. Interestingly, this is not the case for the mean pitching contribution $\overline{C_{P_\theta}}$, although the instantaneous $C_{P_\theta}(t)$ peak does increase with H_0/c. Indeed, when the foil is not ongoing a high-speed reversal, $C_{P_\theta}(t)$ tends toward lower values as H_0/c increases, because the kinematic parameters f^* and α_0 have lower optimal values.

As pointed out in the experimental study by Kim et al. [11], the encounter of an optimal operating frequency is due to the cumulative effect of a heaving contribution increasing with f^* and a pitching contribution decreasing with f^*. Figure 13 shows an example of these contributions in the $f^* - \alpha_0$ parametric space for $H_0/c = 5$. The highest $\overline{C_{P_Y}}$ is always found at the highest value of f^*, whereas the less negative $\overline{C_{P_\theta}}$ is found at the lowest f^*, and vice versa, for all heaving amplitudes studied. However, the occurrence of well-timed LEVS disrupts the uniformity of the $\overline{C_{P_\theta}}$ distribution for $H_0/c = 1$ and $H_0/c = 3$, which features positive values leading to secondary peaks in the efficiency contours shown in Figs. 7 and 8.

For a fixed frequency and heaving amplitude, the optimization of the amplitude of the angle of attack, the α_0 parameter, mainly allows

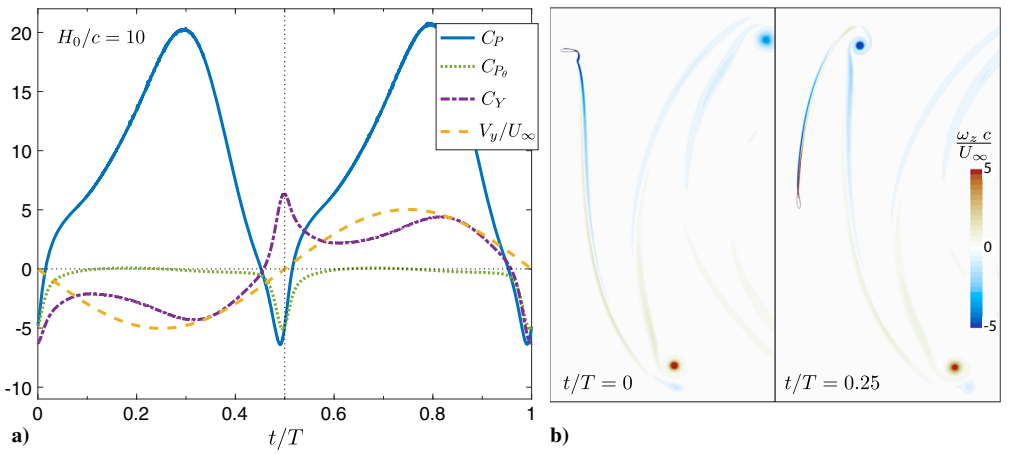

Fig. 12 a) Instantaneous power contributions and b) vorticity field for the most efficient case with sinusoidal $\alpha(t)$ at $H_0/c = 10$, that is, $f^* = 0.08$ and $\alpha_0 = 18°$.

to modify the shape of C_Y and improve the synchronization of its peak with the maximum heaving velocity $\hat{V}_y$, at $t/T = 0.25$ and 0.75, and thus increase $\overline{C_{P_Y}}$. A higher α_0 has not been found to be directly related to higher C_Y or C_{P_θ} values, although it does systematically increase the drag of the turbine, C_X. This is also the case for an increase in frequency or in heaving amplitude with other parameters fixed, as expected.

D. Optimization Through Further Tuning of the Effective Angle-of-Attack Function

As seen in the results so far, a prescribed sinusoidal effective angle of attack is suitable to high heaving amplitude cases; however, it is not necessarily an optimal shape function.

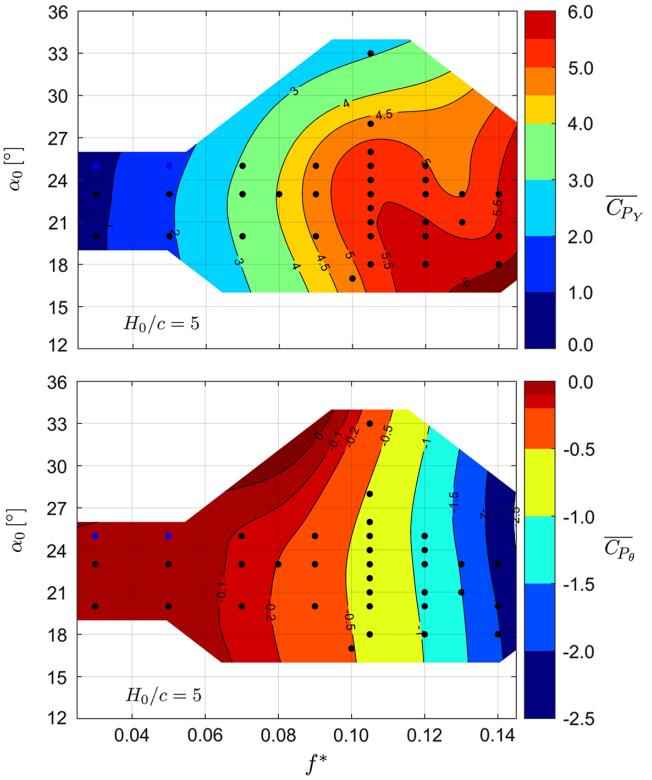

Fig. 13 Distribution of the heaving and pitching power contributions in the $f^* - \alpha_0$ parametric space for $H_0/c = 5$.

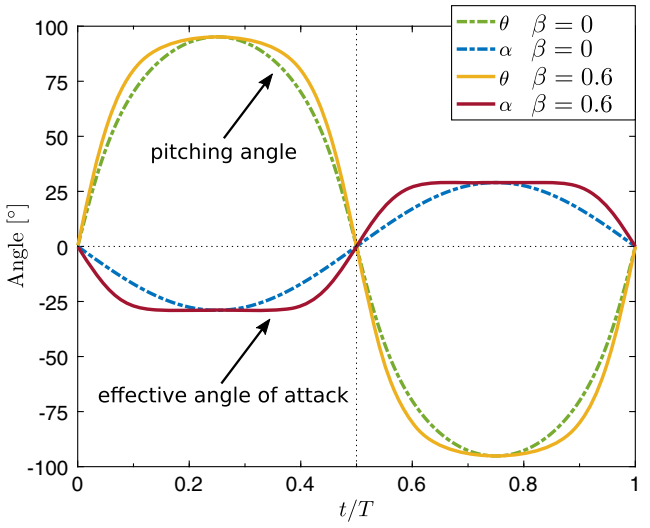

Fig. 14 Impact of the β parameter on the instantaneous pitching angle and effective angle of attack.

Table 4 Effect of increasing the β parameter on the performance metrics of the most efficient cases presented in Table 3

H_0/c	f^*	α_0, °	β	$\overline{C_X}$	$\overline{C_{P_\theta}}$	$\overline{C_P}$	η, %
3	0.12	27	0	5.320	−0.588	3.000	44.8
3	0.12	27	**0.6**	6.179	−0.714	3.152	46.8
5	0.105	21	0	8.020	−0.640	4.810	44.9
5	0.105	21	**1.0**	9.303	−0.957	5.196	47.9
10	0.08	18	0	15.424	−0.547	9.214	44.5
10	0.08	18	**1.0**	17.585	−0.743	10.196	49.0
15	0.07	15	0	22.765	−0.544	13.489	43.9
15	0.07	15	**1.0**	25.839	−0.727	15.083	49.0

Bold values of β correspond to the new, improved cases with respect to the original cases of Table 3.

A new function is therefore proposed in this work to prescribe the angle of attack as:

$$\alpha(t) = -\alpha_0 \sin(\omega t + \beta \sin(2\omega t)) \tag{12}$$

where α_0 is the angle of attack amplitude and β is a shape parameter that flattens the $\alpha(t)$ profile around its peak value compared with a sinusoidal profile ($\beta = 0$). This is shown in Fig. 14. To obtain the desired α profile, the expression of the modified pitching function is derived from Eqs. (1), (3), and (12):

$$\theta(t) = \arctan\left(-\frac{\omega H_0}{U_\infty}\cos(\omega t + \phi)\right) + \alpha_0 \sin(\omega t + \beta \sin(2\omega t)) \tag{13}$$

Flattening the $\alpha(t)$ profile around its peak value is usually beneficial for large heaving amplitude cases as shown in Table 4, where the best cases found for sinusoidal angle of attack ($\beta = 0$) are further improved when using $\beta = 0.6$ or 1.

The dashed lines in Fig. 15 provide an example of the impact of increasing the β parameter for a highly-efficient case at large heaving amplitude, where it has been observed to be beneficial to the efficiency. The modified α profile, with higher values around $t/T = 0.1$ and $t/T = 0.4$ (see Fig. 14), leads to an increase in C_Y. This results in a fuller $C_P(t)$ profile and a higher overall energy extraction, at the expense of a more negative $\overline{C_{P_\theta}}$ with a higher peak value during the reversals. Sustaining a large angle of attack, along with the more aggressive reversals, also increases the risks of dynamic stall. Indeed, using $\beta = 1$ with the optimal case at $H_0/c = 3$ has been found to trigger unsynchronized LEVS, hence the use of a lower value $\beta = 0.6$

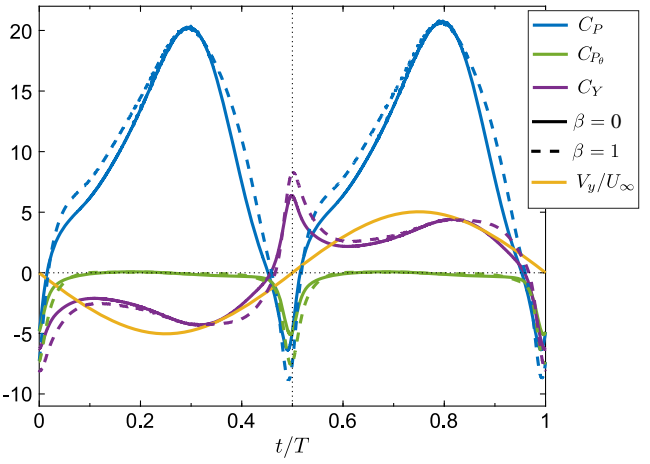

Fig. 15 Comparison of the instantaneous power contributions for sinusoidal ($\beta = 0$, $\eta = 44.5\%$, solid lines) and modified ($\beta = 1$, $\eta = 49.0\%$, dashed lines) angle-of-attack evolutions. $H_0/c = 10$, $f^* = 0.08$, and $\alpha_0 = 18°$.

for the case featured in Table 4 at this heaving amplitude. At $H_0/c = 1$, the use of a positive β parameter does not improve the efficiency, rather leading to unsynchronized LEVS for cases that performed well without LEVS, and deteriorating the synchronization for cases with well-timed LEVS. The relative gain in efficiency made with $\beta > 0$ increases with the heaving amplitude, reaching 12% at $H_0/c = 15$, and thus allowing to reach an impressive $\eta = 49.0\%$, the highest efficiency observed in this study.

IV. Conclusions

Before this study, only relatively small heaving amplitudes had been considered for oscillating-foil turbines, and optimal operating conditions had mostly been identified with the occurrence of well-timed leading-edge vortex shedding that helped the reversal of the foil. However, experimental and 3D numerical studies showed that it might become challenging to maintain high efficiencies while relying on vortex synchronization for a finite foil with 3D effects at the wing tips.

A modified pitching motion has been proposed to prescribe a sinusoidal angle-of-attack profile, allowing to maintain a high efficiency while increasing the heaving amplitudes. Efficient cases without leading-edge vortex shedding (LEVS) at the low heaving amplitude of $H_0/c = 1$ have also been identified. The optimal cases have been used to investigate the impact of a β parameter that further modifies the angle-of-attack profile, allowing to achieve efficiencies of up to 49% at $H_0/c = 15$, the highest heaving amplitude studied, corresponding to a mean power extraction of $\overline{C_P} = 15.0$. Indeed, optimizing the operating conditions for every value of H_0/c has allowed to maintain an increase of the extracted power proportional to that of the swept area. However, the higher translating and rotating velocities of the foil induced by larger heaving amplitudes, along with the reduced optimal operating range, suggest that these high efficiencies may be challenging to achieve in practice with regard to the pitch controller required.

The new range of motions explored hereby, namely, an angle-of-attack-governed pitching motion combined with a high-amplitude heaving motion, could greatly increase the power extracted by a single oscillating foil, and extend its application to new designs where a relatively small-chord foil can efficiently extract energy from a large window, without depending on well-timed LEVS. It is worth to note that, for a given application in a deployment site, the specific choice of heaving amplitude will depend on design constraints, considerations of turbine optimization versus array optimization as well as economic aspects, which are all beyond the scope of the present paper. Further work is needed.

Acknowledgments

The authors would like to acknowledge access to the high-performance computing resources of Compute Canada as well as the financial support from Natural Sciences and Engineering Research Council of Canada (NSERC Discovery Grant RGPIN-2018-04527) and the French company OmegaWatt. Motivation for this investigation is attributable to monsieur Pierre Fristot, and the authors warmly thank him for that.

References

[1] Young, J., Lai, J. C. S., and Platzer, M. F., "A Review of Progress and Challenges in Flapping Foil Power Generation," *Progress in Aerospace Sciences*, Vol. 67, May 2014, pp. 2–28. https://doi.org/10.1016/j.paerosci.2013.11.001

[2] Xiao, Q., and Zhu, Q., "A Review on Flow Energy Harvesters Based on Flapping Foils," *Journal of Fluids and Structures*, Vol. 46, April 2014, pp. 174–191. https://doi.org/10.1016/j.jfluidstructs.2014.01.002

[3] Kinsey, T., and Dumas, G., "Parametric Study of an Oscillating Airfoil in a Power-Extraction Regime," *AIAA Journal*, Vol. 46, No. 6, 2008, pp. 1318–1330. https://doi.org/10.2514/1.26253

[4] McKinney, W., and DeLaurier, J., "Wingmill: An Oscillating-Wing Windmill," *Journal of Energy*, Vol. 5, No. 2, 1981, pp. 109–115. https://doi.org/10.2514/3.62510

[5] Boudreau, M., Gunther, K., and Dumas, G., "Investigation of the Energy-Extraction Regime of a Novel Semi-Passive Flapping-Foil Turbine Concept with a Prescribed Heaving Motion and a Passive Pitching Motion," *Journal of Fluids and Structures*, Vol. 84, Jan. 2019, pp. 368–390. https://doi.org/10.1016/j.jfluidstructs.2018.11.014

[6] Boudreau, M., Dumas, G., Rahimpour, M., and Oshkai, P., "Experimental Investigation of the Energy Extraction by a Fully-Passive Flapping-Foil Hydrokinetic Turbine Prototype," *Journal of Fluids and Structures*, Vol. 82, Oct. 2018, pp. 446–472. https://doi.org/10.1016/j.jfluidstructs.2018.07.014

[7] Kinsey, T., Dumas, G., Lalande, G., Ruel, J., Mehut, A., Viarouge, P., Lemay, J., and Jean, Y., "Prototype Testing of a Hydrokinetic Turbine Based on Oscillating Hydrofoils," *Renewable Energy*, Vol. 36, No. 6, 2011, pp. 1710–1718. https://doi.org/10.1016/j.renene.2010.11.037

[8] Kinsey, T., and Dumas, G., "Three-Dimensional Effects on an Oscillating-Foil Hydrokinetic Turbine," *Journal of Fluids Engineering*, Vol. 134, No. 7, 2012, Paper 071105. https://doi.org/10.1115/1.4006914

[9] Kinsey, T., and Dumas, G., "Optimal Operating Parameters for an Oscillating Foil Turbine at Reynolds Number 500,000," *AIAA Journal*, Vol. 52, No. 9, 2014, pp. 1885–1895. https://doi.org/10.2514/1.J052700

[10] Drofelnik, J., and Campobasso, M. S., "Comparative Turbulent Three-Dimensional Navier–Stokes Hydrodynamic Analysis and Performance Assessment of Oscillating Wings for Renewable Energy Applications," *International Journal of Marine Energy*, Vol. 16, Dec. 2016, pp. 100–115. https://doi.org/10.1016/j.ijome.2016.05.009

[11] Kim, D., Strom, B., Mandre, S., and Breuer, K., "Energy Harvesting Performance and Flow Structure of an Oscillating Hydrofoil with Finite Span," *Journal of Fluids and Structures*, Vol. 70, April 2017, pp. 314–326. https://doi.org/10.1016/j.jfluidstructs.2017.02.004

[12] Simpson, B., "Experimental Studies of Flapping Foils for Energy Extraction," M.Sc. Thesis, Dept. of Mechanical Engineering, Massachusetts Inst. of Technology, Cambridge, MA, 2009.

[13] Young, J., Ashraf, M. A., Lai, J. C. S., and Platzer, M. F., "Numerical Simulation of Fully Passive Flapping Foil Power Generation," *AIAA Journal*, Vol. 51, No. 11, 2013, pp. 2727–2739. https://doi.org/10.2514/1.J052542

[14] Lu, K., Xie, Y., Zhang, D., and Xie, G., "Systematic Investigation of the Flow Evolution and Energy Extraction Performance of a Flapping-Airfoil Power Generator," *Energy*, Vol. 89, Sept. 2015, pp. 138–147. https://doi.org/10.1016/j.energy.2015.07.053

[15] Kinsey, T., and Dumas, G., "Computational Fluid Dynamics Analysis of a Hydrokinetic Turbine Based on Oscillating Hydrofoils," *Journal of Fluids Engineering*, Vol. 134, No. 2, 2012, Paper 021104. https://doi.org/10.1115/1.4005841

[16] Spalart, P. R., and Allmaras, S. R., "A One-Equation Turbulence Model for Aerodynamic Flows," *Recherche Aérospatiale*, No. 1, 1994, pp. 5–21.

[17] Dacles-Mariani, J., Zilliac, G. G., Chow, J. S., and Bradshaw, P., "Numerical/Experimental Study of a Wingtip Vortex in the Near Field," *AIAA Journal*, Vol. 33, No. 9, 1995, pp. 1561–1568. https://doi.org/10.2514/3.12826

[18] Gauthier, E., Kinsey, T., and Dumas, G., "Impact of Blockage on the Hydrodynamic Performance of Oscillating-Foils Hydrokinetic Turbines," *Journal of Fluids Engineering*, Vol. 138, No. 9, 2016, Paper 091103. https://doi.org/10.1115/1.4033298

H. Dong
Associate Editor